# Catalysis Science & Technology

## Accepted Manuscript

This article can be cited before page numbers have been issued, to do this please use: Y. Feng, C. Lu, H. Wang, M. Meng, Y. Zhang, D. Rao, L. Liu and H. Yin, *Catal. Sci. Technol.*, 2020, DOI: 10.1039/D0CY01733G.

ROYAL SOCIETY
OF **CHEMISTRY**

rsc.li/catalysis

View Article Online
DOI: 10.1039/D0CY01733G

Received 00th January 20xx,
Accepted 00th January 20xx

DOI: 10.1039/x0xx00000x

# Spinel copper-iron-oxide magnetic nanoparticles with cooperative Cu(I) and Cu(II) sites for enhancing catalytic transformation of 1,2-propanediol to lactic acid under anaerobic conditions

Yonghai Feng,*[a] Congming Lu,[a] Huijie Wang,[a] Minjia Meng,[b] Yunlei Zhang, [b] Dewei Rao,*[a] Lei Liu [a] and Hengbo Yin [b]

The aerobic catalytic oxidation of 1,2-propanediol (PDO) over non-noble metal (eg. Cu) based catalysts usually suffers serious C3 product dissociation at high temperature, thus showing low lactic acid (LA) selectivity. Here, an alternative anaerobic catalysis strategy over spinel copper-iron-oxide magnetic nanoparticles ($CuFeO_x$ MNs) with coexistence of Cu(I) and Cu(II) dual sites is developed for the catalytic transformation of PDO to LA with a quantitative yield of co-product $H_2$ in basic aqueous solution. The absence of $O_2$ is beneficial for enhancing LA production in comparison with the presence of $O_2$. Synergy between Cu(I) and Cu(II) sites in $CuFeO_x$ MNs is vital for improving the catalytic performance as compared to $Cu_2O$ or CuO catalysts with Cu(I) or Cu(II) sites alone. $Cu_1Fe_1O_x$ MNs with Cu/Fe mole ratio of 1/1 exhibits 94.5% LA selectivity and 72.6% PDO conversion at 160℃ for 8 h. Experimental results and DFT calculations suggest that the spinel $CuFeO_x$ MNs based catalytic PDO transformation follows a favorable pathway of PDO → hydroxyacetone → lactaldehyde → lactic acid for LA production. In addition to the catalytic PDO transformation, the $CuFeO_x$ MNs can be extended to favor high activity and selectivity in the catalytic transformation of glycerol to LA (98.5% selectivity) and ethylene glycol to glyceric acid (97.8% selectivity). This work highlights the design of an alternative non-noble metal based $CuFeO_x$ MNs catalyst for efficiently catalyzing the transformation of bio-based polyols into value-added carboxyl acids.

## Introduction

The conversion of renewable biomass derivatives to liquid fuels, chemicals, and polymeric materials attracts great interest for its potential to replace petroleum as the primary feedstock.[1, 2] 1,2-propanediol (PDO), a bio-based diol with vicinal primary and secondary alcohol groups, has been emerged as an alternative promising platform chemical for producing several high value chemicals such as lactic acid (LA), pyruvic acid, propylene epoxide, hydroxylacetone, and pyruvaldehyde *via* catalytic processes.[3] LA has potential as a major feedstock for sustainably producing several important commodity chemicals such as biodegradable fibres, polylactic acid esters, and acrylic acid.[4] It is estimated over 90% of global LA is mainly produced by the carbohydrate fermentation route, which however is slow and involves complex separation steps with a large amount of sludge generation.[5] In this case, it is attractive to develop the selective conversion of PDO as an economic and environmental friendly approach for the sustainable production of LA.

To date, studies on the PDO conversion to LA are mainly focused on $O_2$-required thermal catalysis or electronic catalysis approaches using supported noble metal (Au, Pd, and Pt) nanoparticles as catalysts due to their high LA selectivity.[5-11] For examples, monometallic Au/C catalyst can selectively catalyse the oxidation of PDO to LA at 90℃ and 0.3 MPa $O_2$, giving 100% LA selectivity and 78% PDO conversion,[6] while bimetallic AuPd/C and AuPt/C catalysts are more active, giving the PDO conversion and LA selectivity of higher than 94% and 95%, respectively at 60℃ and 1 MPa $O_2$.[10] Chadderdon et al. has recently developed the selective oxidation of PDO in alkaline anion-exchange membrane electrocatalytic flow reactors, giving the LA selectivity of 86.8% over carbon-supported platinum (Pt/C) Pt/C catalyst.[5] In view of the high cost of noble metal, non-noble/noble bimetallic catalysts such as the Cu@Au core shell nanoparticles and the $AuCu/TiO_2$ catalysts have recently been developed for the selective oxidation of PDO to LA,[12, 13] in which however the active sites still depend on gold. Inexpensive metallic Ag and Cu nanoparticles are tried to be developed as catalyst for the PDO oxidation,[14, 15] but higher reaction temperature is required to activate the reaction due to their inherent low catalytic activity. Consequently, severe scission of C–C bond of C3 intermediates to C1 and C2 products occurs, leading to low LA selectivity. For

---

[a] *Institute for Advanced Materials, School of Materials Science and Engineering, Jiangsu University, Zhenjiang 212013, China.*
[b] *School of Chemistry and Chemical Engineering, Jiangsu University, Zhenjiang 212013, China.*
**Corresponding authors: Y. Feng (fengyonghai@ujs.edu.cn), D. Rao (dewei@ujs.edu.cn)*

Electronic Supplementary Information (ESI) available: [description of DFT methods, supporting figures and tables]. See DOI: 10.1039/x0xx00000x

View Article Online
DOI: 10.1039/D0CY01733G

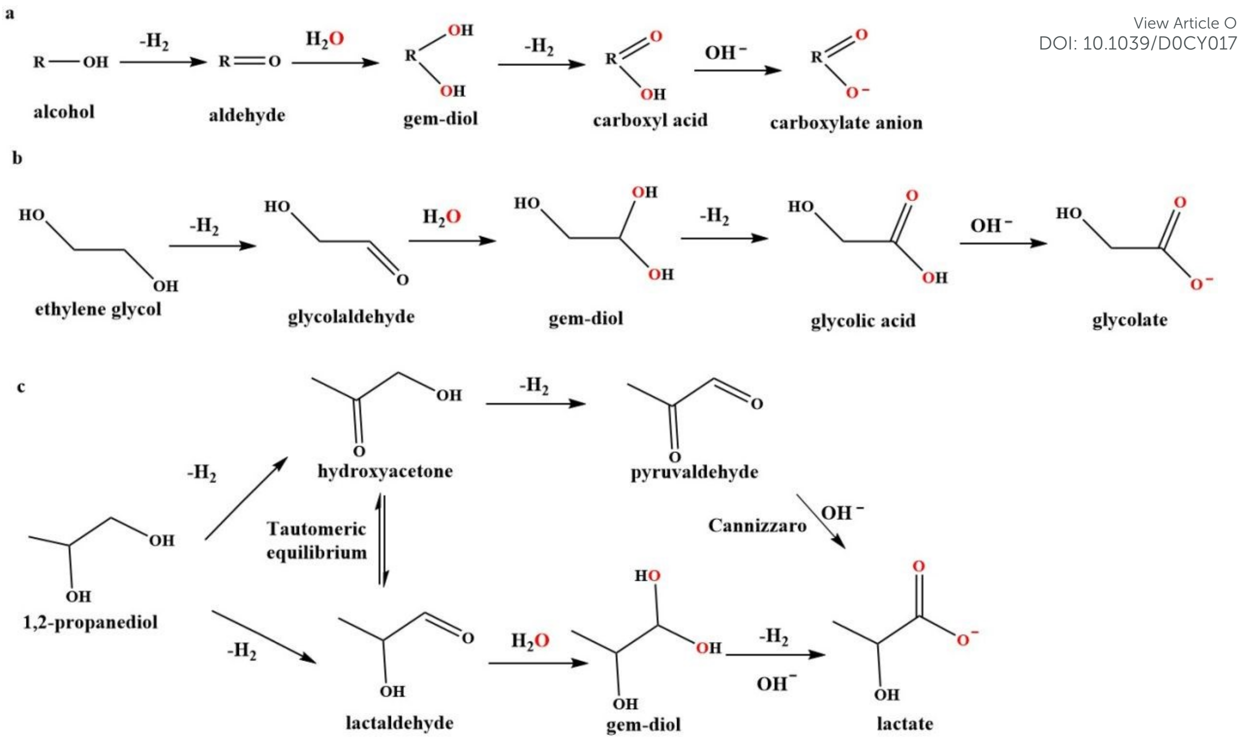

**Scheme 1.** Reaction pathways for catalytic transformation of alcohols to carboxyl acid (a) and ethylene glycol to glycolic acid (b) using water as oxygen source in basic aqueous solution with $H_2$ as co-product. Reaction network of $O_2$-required catalytic oxidation of PDO to LA (c).

instance, using metallic $Cu^0$ nanoparticles as catalyst displays LA selectivity of only 52.4% and total selectivities of formic acid (C1 product) and acetic acid (C2 product) of 48% at the PDO conversion of 83.8% under 1 MPa $O_2$ and 200 ℃.[15] In addition, the high pressurized dioxygen (1−2 MPa $O_2$) and high temperature (200−220 ℃) will also pose a great risk for practical production. To address these issues, alternative safe approaches that can also efficiently promote the LA selectivity especially over non-noble metal based catalysts need to be developed.

Previous works have shown that alcohols can be catalytically transformed into corresponding carboxyl acid salt and $H_2$ using water as oxygen atom source in basic aqueous solution (Scheme 1a).[16, 17] Haasterecht et al. have found that carbon nanofiber supported copper nanoparticles can selectively catalyse the transformation of ethylene glycol into glycolic acid with $H_2$ as co-product (96% selectivity at 82% conversion) under anaerobic aqueous conditions (Scheme 1b).[18] As shown in the reaction network of aerobic catalytic oxidation of PDO to LA (Scheme 1c), oxygen ($O_2$) is not the actual oxygen atom source for LA formation even its presence was believed to be able to promote the PDO conversion.[19] On basis of the fact that alcohols and ethylene glycol can be selectively transformed into their corresponding carboxyl acid under anaerobic and basic aqueous conditions, we believe that this $O_2$-free catalysis system may be extended to selectively catalyse the PDO transformation into LA over non-noble metal based catalysts. To achieve this goal, the priority is to explore the desirable catalysts. Moreover, one should be noticed that the reaction pathway for PDO conversion is complex, so the mechanism of catalytic transformation of PDO to LA is worth being clarified, in particular, for the new designed catalysts.

Recently, copper ferrite ($CuFe_2O_4$) magnetic nanoparticles (MNs) have emerged as one of the most attractive catalysts for oxidative dehydrogenation of alcohols to their corresponding carbonyl compounds due to its cation occupying the tetrahedral and octahedral holes in a dense cubic packing of oxygen anions.[20-22] Moreover, the spinel structure of $CuFe_2O_4$ is stable and highly ordered, which can maintain their promising activities in harsh conditions. However, the catalytic performance of $CuFe_2O_4$ MNs for the catalytic transformation of PDO under anaerobic and basic aqueous solution remains unclear. It has been reported that $Cu_2O$ is more active and selective than $Cu^0$ and CuO in catalytic transformation of glycerol to LA in alkaline medium.[23] Therefore, a novel type of spinel copper-iron-oxide magnetic nanoparticles ($CuFeO_x$ MNs) with coexistence of Cu(I) and Cu(II) sites was synthesized by the facile high-temperature organic phase synthesis approach,[24] and used for catalytic PDO transformation under anaerobic and basic aqueous solution in order to improve the LA selectivity over non-precious metal based catalysts. It was found that under anaerobic condition C−C bond dissociation reaction could be effectively hindered as compared to that under aerobic condition, thereby high LA selectivity was achieved with value-added $H_2$ as co-product. The synergy between Cu(I) and Cu(II) centres in the $CuFeO_x$ MNs was suggested to contribute to the enhanced catalytic performance. By tailoring the Cu/Fe ratio to 1/1 in $CuFeO_x$ ($Cu_1Fe_1O_x$) MNs, 94.5% LA selectivity and 72.6% PDO conversion was obtained at 160℃ and 1.0 MPa $N_2$ for 8 h. The pathway of catalytic PDO transformation over $CuFeO_x$ MNs is

View Article Online
DOI: 10.1039/D0CY01733G

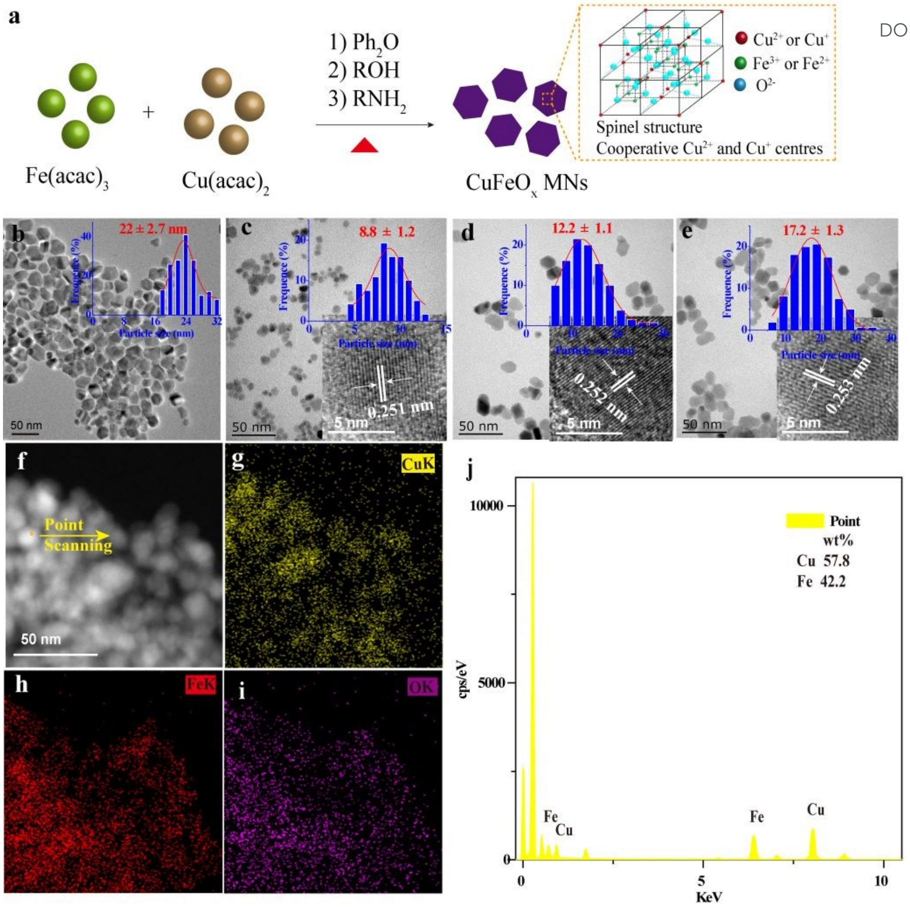

**Fig. 1.** Schematic illustration of the preparation of spinel CuFeO$_x$ MNs (a); TEM and HRTEM images of Fe$_3$O$_4$ (b), Cu$_{0.5}$Fe$_1$O$_x$ (c), Cu$_1$Fe$_1$O$_x$ (d), and Cu$_2$Fe$_1$O$_x$ (e); HAADF-STEM image of Cu$_1$Fe$_1$O$_x$ MNs (f), element mappings of Cu (g), Fe (h), O (i); corresponding EDS spectrum of one particle.

investigated through experiments and density functional theory (DFT) calculation. Interestingly, the CuFeO$_x$ MNs also display high activity in selectively catalysing glycerol transformation to LA (98.5% selectivity) and ethylene glycol to glyceric acid (97.8% selectivity). Moreover, the CuFeO$_x$ MNs can be facilely recovered by magnetic separation with promising stability.

## Results and discussion

### Synthesis of CuFeO$_x$ MNs and characterizations

Hexagonal-like monodisperse CuFeO$_x$ MNs with spinel structure could be facilely synthesized using Cu(II) acetylacetonate (Cu(acac)$_2$) and iron (III) acetylacetonate (Fe(acac)$_3$) as copper and iron precursor, respectively in mixture of phenyl ether (Ph$_2$O), alcohol (ROH), and oleylamine (RNH$_2$) solution at temperature of 300℃, as depicted in Fig. 1a. Owing to the reduction by oleylamine, partial Cu$^{2+}$ ions were converted into Cu$^+$ species in the framework of CuFeO$_x$ MNs, similar to the partial reduction of Fe$^{3+}$ ions to Fe$^{2+}$ ions.[24] Fig. 1b–e shows the TEM images of as-synthesized CuFeO$_x$ MNs based on Ni grids. It is noting that CuFeO$_x$ MNs are mainly irregular hexagonal-like nanoparticles, similar to the morphology of pristine Fe$_3$O$_4$ MNs (Fig. 1b). The obtained CuFeO$_x$ MNs are nearly monodisperse with a narrow size distribution range. The sizes of Cu$_{0.5}$Fe$_1$O$_x$, Cu$_1$Fe$_1$O$_x$, and Cu$_2$Fe$_1$O$_x$ MNs are ca. 7.4, 12.2, and 17.2 nm, respectively, indicating that increasing the Cu/Fe mole ratio favors forming larger-sized CuFeO$_x$ MNs. Corresponding HRTEM images

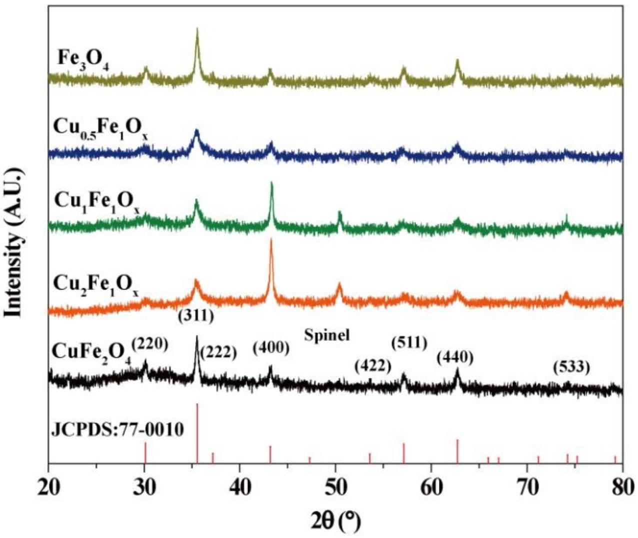

**Fig. 2.** XRD spectra of CuFeO$_x$ MNs with different Cu/Fe ratios.

View Article Online
DOI: 10.1039/D0CY01733G

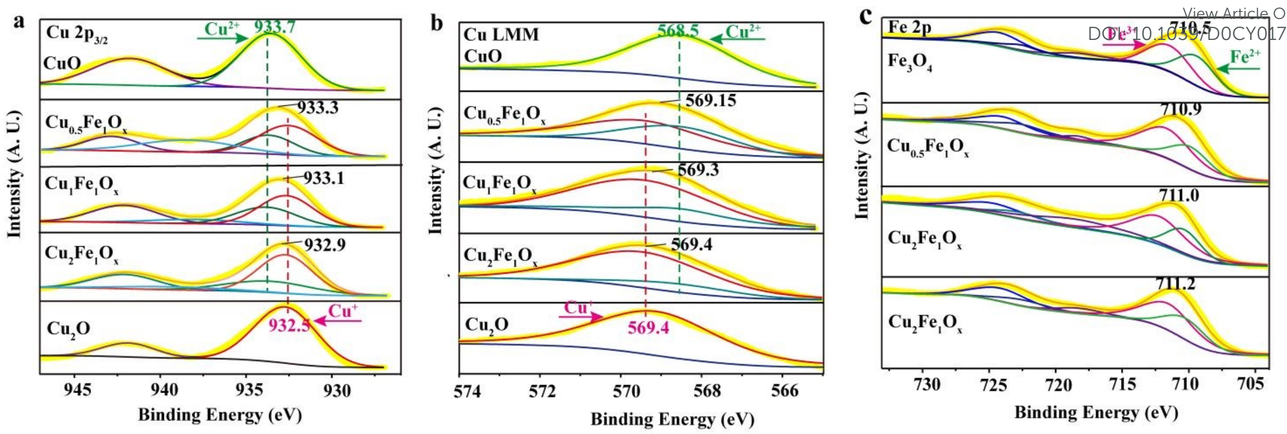

**Fig. 3.** XPS spectra of Cu $2P_{3/2}$ (a), Cu LMM (b), and Fe 2p (c) of $CuFeO_x$ MNs with CuO and $Cu_2O$ as comparison.

(insets of Fig. 1c–e) show that the lattice fringes of $Cu_{0.5}Fe_1O_x$, $Cu_1Fe_1O_x$, and $Cu_2Fe_1O_x$ MNs are examined to 0.251, 0.252, and 0.253 nm, respectively, similar to the (311) lattice spacing of spinel copper ferrite ($CuFe_2O_4$),[25] in which the Cu ions sit predominantly on tetrahedral sites and iron atoms on octahedral sites (as depicted in Fig. 1a). Fig. 1f–i is the HAADF-STEM image and corresponding element mapping of $Cu_1Fe_1O_x$ MNs. The Cu, Fe, and O elements (Fig. 1g-i) are detected in the selected region, and their distributions are homogeneous, indicating that these materials are well crystallized [15]. And the detail element ratio of Cu/Fe is displayed in Fig. 1j measured by the point scanning EDS spectrum of one particle, indicating the similar Cu/Fe ratio (wt. %) to the given amount.

To explore the crystal properties of our prepared samples, the XRD is common method. Fig. 2 clearly shows that the copper ferrite ($CuFe_2O_4$), prepared by hydrothermal method (its morphology is described in Fig. S2), exhibits the typical XRD patterns of cubic spinel structure, of which the peaks at $2\vartheta$= 30.0, 35.5, 43.2, 53.4, 57.3, 62.6, and 74.3° can be ascribed to the (220), (311), (222), (400), (422), (511), (440), and (533) crystal planes of the copper ferrite (JCPDS 77-0010), respectively.[26] As for the $Cu_{0.5}Fe_1O_x$ MNs with similar Cu/Fe ratio (0.5) to $CuFe_2O_4$, its apparent characteristic peaks are consistent with those of $CuFe_2O_4$, meaning that it possesses the cubic spinel structure, in accordance with the HRTEM analysis (Fig. 1c). In case of $Cu_1Fe_1O_x$ and $Cu_2Fe_1O_x$ MNs with the Cu/Fe ratios of 1.0 and 2.0, respectively, the XRD patterns are similar to that of $Cu_{0.5}Fe_1O_x$ MNs, which indicates that both the $Cu_1Fe_1O_x$ and $Cu_2Fe_1O_x$ MNs also possess the good cubic spinel structure although they have a much higher copper content (2 or 4 times), in accordance with the HRTEM analysis (Fig. 1d and e). Nevertheless, for the profiles of $Cu_1Fe_1O_x$ and $Cu_2Fe_1O_x$ MNs, the intensity of the peak at $2\vartheta$ = 43.2° is obviously enhanced and a new peak at $2\vartheta$ = 50.5° appears, suggesting that reduced copper species (eg. $Cu^0$, JCPDS 85-1326) might be formed in the matrix of $CuFeO_x$ MNs.[27] This may be due to that $CuFeO_x$ MNs have high copper contents will lead to more $Cu^{2+}$ species reduced by oleylamine and alcohol at high temperature. It should be noted that the actual oxidation state of reduced copper species exposed on the surface of $CuFeO_x$ MNs should be further confirmed by X-ray photoelectron spectroscopy (XPS) and Auger electron spectroscopy (AES) analysis (as discussed in the following section). The crystalline sizes based on the (311) plane of the MNs are in an order of $Cu_{0.5}Fe_1O_x$ (8.2 nm) < $Cu_1Fe_1O_x$ (10.4 nm) < $Cu_2Fe_1O_x$ (16.8 nm) < $Fe_3O_4$ (19.7 nm) (Table 1), consistent with that of TEM analysis.

XPS studies were conducted for elucidating the surface constitution/elemental chemical states of $CuFeO_x$ MNs with different Cu/Fe ratios, as shown in Fig. 3. For the core level XPS of Cu 2p regions, the binding energy of Cu $2p_{3/2}$ is located at 933.0 eV with a satellite peak at 942.1 eV, revealing that the Cu oxidation state is +2 with a $d^9$ electron configuration in $CuFeO_x$ MNs.[28] The binding energies of the $Cu2p_{3/2}$ peaks for $CuFeO_x$ MNs are in the order of $Cu_{0.5}Fe_1O_x$ (933.2 eV) < $Cu_1Fe_1O_x$ (933.1 eV) < $Cu_2Fe_1O_x$ (932.9 eV). As the copper content increases, the $Cu2p_{3/2}$ peak shifts to lower binding energy, accompanying with the declined intensity of the satellite peak, which suggest that more $Cu^{2+}$ species are reduced as reduced copper species ($Cu^+$ or $Cu^0$) have lower binding energy. The $Cu2p_{3/2}$ peak of the three $CuFeO_x$ MNs sample can be deconvoluted into two obvious peaks at 933.7 and 932.5 eV, which are similar to the characteristic peaks of single CuO (933.7 eV) and $Cu_2O$ (932.5 eV), respectively,[28] revealing that $Cu^{2+}$ (933.7 eV) and $Cu^+$ (932.5 eV) species may be coexisted on $CuFeO_x$ MNs surface. The area ratios of peak at 932.5 eV ($Cu^+$) to peak at 933.7 eV ($Cu^{2+}$) for $Cu_{0.5}Fe_1O_x$, $Cu_1Fe_1O_x$, and $Cu_2Fe_1O_x$ are 1.5, 1.6, and 1.8, respectively, suggesting that more copper species are reduced for $CuFeO_x$ with higher copper content. As well known that Cu $2p_{3/2}$ XPS of $Cu^+$ and $Cu^0$ are hardly differentiated,[29] Auger Cu LMM spectra of $CuFeO_x$ MNs (Fig. 3b) are employed to investigate their differences. As for single CuO and $Cu_2O$, the Cu LMM spectra exhibit the characteristic peaks at 568.5 and 569.4 eV, respectively. In case of $CuFeO_x$ MNs, the Cu LMM peaks can be deconvoluted into two peaks at 568.5 and 569.4 eV, assigned to $Cu^{2+}$ and $Cu^+$, respectively, and no characteristic peak for $Cu^0$ species (568.0) is observed probably due to the weak reduction capacity of oleylamine and alcohol mixture. The area of peak at 569.4 eV increases with increasing the Cu/Fe ratio, indicating that more $Cu^+$ are formed in $CuFeO_x$ MNs with higher copper content, contributing to the Cu LMM peak shift

View Article Online
DOI: 10.1039/D0CY01733G

**Table 1** Physicochemical properties of CuFeOx MNs with different Cu/Fe ratios

| Samples | Metal content[a] (wt%) | | $S_{BET}$[b] ($m^2 g^{-1}$) | Crystalline Size[c] (nm) | Mean particle size[d] (nm) | Atom ratio[e] (%) | | | $A_{Cu(I)/Cu(II)}$[f] | | Surface Cu dispersion (D%)[g] | Ms[h] (emu $g^{-1}$) |
|---|---|---|---|---|---|---|---|---|---|---|---|---|
| | Cu | Fe | | | | Cu | Fe | O | $Cu_{2p3/2}$ | $Cu_{LMM}$ | | |
| $Fe_3O_4$ | 0 | 22.6 | 60.3 | 19.7 | 22.0 | 0 | 25.2 | 74.8 | - | - | - | 74.0 |
| $Cu_{0.5}Fe_1O_x$ | 10.2 | 20.2 | 61.2 | 8.2 | 8.8 | 15.5 | 27.2 | 57.3 | 1.5 | 1.6 | 0.20 | 53.0 |
| $Cu_1Fe_1O_x$ | 18.5 | 16.9 | 47.8 | 10.4 | 12.2 | 18.9 | 19.8 | 61.3 | 1.6 | 2.5 | 0.10 | 41.0 |
| $Cu_2Fe_1O_x$ | 26.1 | 15.9 | 32.4 | 16.8 | 17.2 | 22.6 | 19.7 | 57.7 | 1.8 | 5.7 | 0.14 | 28.0 |

[a] The actual metal content was calculated by ICP.

[b] $S_{BET}$ represents the specific surface area calculated by BET method based on $N_2$ adsorption and desorption characterization.

[c] The crystalline size of the (311) plane of $CuFeO_x$ MNs was calculated by the Scherrer equation based XRD pattern.

[d] The mean particle size was measured based on TEM image.

[e] The atom ratio of Cu, Fe, and O of the samples were detected by XPS.

[f] The $A_{Cu(I)/Cu(II)}$ represents the area ratio of deconvoluted peaks associated with $Cu^+$ and $Cu^{2+}$, respectively in $Cu2p_{3/2}$ and CuLMM spectra.

[g] Surface Cu dispersion (D%) was calculated by CO pulse chemisoportion.

[h] The Ms represents the magnetization saturation value.

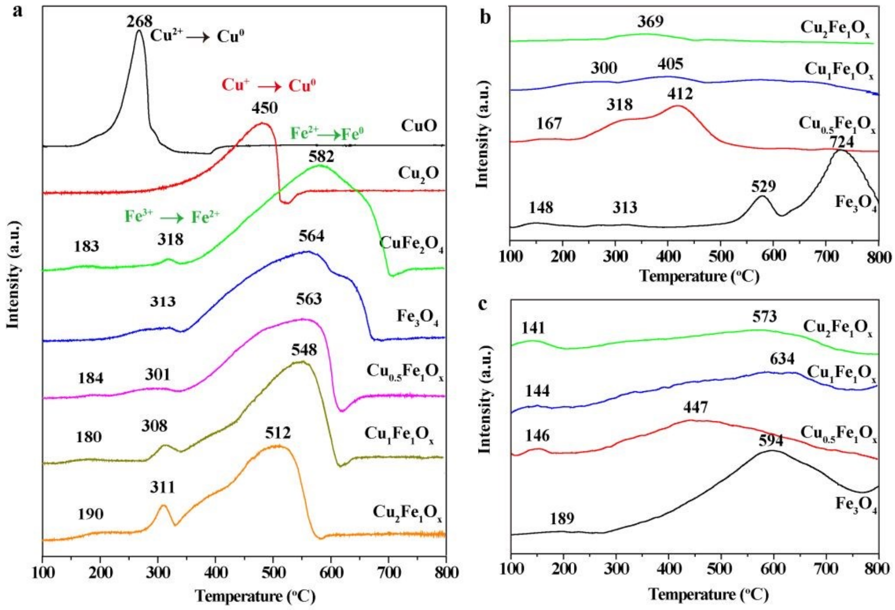

**Fig. 4.** Profiles of $H_2$-TPR (a), $NH_3$-TPD (b), and $CO_2$-TPD (c) of $CuFeO_x$ MNs.

to higher binding energy. In general, the Cu $2p_{3/2}$ core XPS and Cu LMM Auger transitions results indicate that the copper species exposed on $CuFeO_x$ MNs surfaces are mainly present as $Cu^{2+}$ and $Cu^+$. The Fe 2p spectrum of $Fe_3O_4$ shows five deconvoluted peaks (Fig. 3c), in which the photoelectron peaks at 712.1 and 710.2 eV can be assigned to the $2p_{3/2}$ of the $Fe^{3+}$ ion and $Fe^{2+}$ ion, respectively.[30] The presence of a satellite peak at 718.5 eV indicates the coexistence of $Fe^{3+}$ and $Fe^{2+}$.[30] For the Fe 2p spectra of $CuFeO_x$ MNs, similar peaks can be deconvoluted, which indicate the coexistence of $Fe^{3+}$ and $Fe^{2+}$. Comparing with $Fe_3O_4$ MNs, the Fe $2p_{3/2}$ peaks of $CuFeO_x$ MNs shift to high binding energy, suggesting the strong interaction between the copper and ion species. The reduced Fe and Cu in our samples should be beneficial for the catalytic processes.

The $NH_3$ and $CO_2$-TPD were used to probe the surface acid-base sites of $CuFeO_x$ MNs since the acid–base sites strongly relate to the catalytic performance for dehydrogenation of alcohol.[31] Considering that PDO is a diol and the initial dehydrogenation of PDO can be rate-step for its transformation to lactic acid,[7, 9, 19, 32] the surface acidity and basicity of $CuFeO_x$ MNs are worthy being studied. As shown in Fig. 4b, the $NH_3$-TPD profile of $Fe_3O_4$ NMs exhibits four desorption peaks with the maximal temperatures ($T_M$) in regions of 100–200, 250–350, 500–800℃, identified as the weak, medium, and strong acid site,[33] respectively, in which the strong acid site originated from the $Fe^{3+}$ and $Fe^{2+}$ ions (Lewis acid site, which is denoted as $\delta^+$.) is dominant (Table S2). In contrast, for $Cu_{0.5}Fe_1O_x$ MNs, the desorption peak of strong

View Article Online
DOI: 10.1039/D0CY01733G

**Table 2.** $O_2$-free catalytic conversion of PDO to LA using different copper based catalysts[a]

| Catalysts | CO uptakes (mmol $g_{cat.}^{-1}$) | Surface copper dispersion[b] (wt%) | Surface copper concentration[c] (mmol $g_{cat.}^{-1}$) | PDO conversion[d] (%) | Selectivities[e] (%) | | | | | LA yield[f] (%) | TOF[g] ($h^{-1}$) |
|---|---|---|---|---|---|---|---|---|---|---|---|
| | | | | | LA | AA | FA | PA | HA | | |
| - | - | - | - | 3.2 | 80.5 | 10.5 | 5.9 | 2.3 | 0.8 | 2.6 | - |
| $Fe_3O_4$ | ND | ND | ND | 4.2 | 79.8 | 10.8 | 6.6 | 2.1 | 0.7 | 3.4 | - |
| $Cu_{0.5}Fe_1O_x$ | 0.030 | 0.20 | 0.0312 | 58.1 | 92.1 | 3.2 | 2.1 | 2.6 | 1.0 | 53.5 | 462 |
| $Cu_1Fe_1O_x$ | 0.016 | 0.10 | 0.0156 | 72.6 | 94.5 | 2.6 | 0.8 | 1.6 | 0.5 | 68.6 | 1410 |
| $Cu_2Fe_1O_x$ | 0.022 | 0.14 | 0.0219 | 68.6 | 90.7 | 4.2 | 2.9 | 1.4 | 0.8 | 62.2 | 895 |
| $Cu_2O$ | 0.038 | 0.24 | 0.0375 | 66.5 | 74.2 | 16.8 | 8.3 | 0.4 | 0.3 | 49.3 | 420 |
| CuO | 0.041 | 0.26 | 0.0406 | 38.3 | 83.5 | 6.4 | 3.3 | 5.0 | 1.8 | 32.0 | 273 |
| $CuFe_2O_4$ | 0.028 | 0.18 | 0.0281 | 43.6 | 88.6 | 4.0 | 2.8 | 3.2 | 1.4 | 38.6 | 427 |
| o-$Cu_1Fe_1O_x$[h] | 0.017 | 0.11 | 0.0172 | 50.2 | 89.4 | 3.8 | 2.2 | 2.8 | 1.8 | 46.4 | 760 |

[a] Reaction conditions: PDO concentration = 0.2 M (40 mL), NaOH/PDO (mol/mol) = 2, reaction temperature = 160℃, $N_2$ = 1.0 MPa, catalyst loading = 0.06 g, reaction time = 8 h.

[b-c] Surface copper ($Cu^+$ and $Cu^{2+}$) dispersion and concentration is calculated on the basis of the results of CO pulse chemisorption.

[d] The PDO conversion is calculated by GC.

[e] The product selectivity is calculated by HPLC. PDO = 1,2-propanediol, LA = lactic acid, AA = acetic acid, FA = formic acid, PA = pyruvic acid, HA = hydroxyacetone.

[f] The LA yield is calculated by PDO conversion multiplied by LA selectivity.

[g] Activity expressed as turnover frequency (TOF) which is based on the number of surface copper and PDO conversion at initial 1 h with PDO conversions of lower than 20% (Fig. S3).

[h] The o-$Cu_1Fe_1O_x$ MNs represents that the $Cu_1Fe_1O_x$ MNs treated at 450℃ with a $O_2$ flow rate of 50 mL $min^{-1}$ for 1 h.

acid site shifts to lower temperature (300–450 ℃) and the concentration of medium acid site is significantly enhanced, which can be attributed to the introduction of copper ions ($Cu^{2+}$ or $Cu^+$), of which the Lewis acid strength is weaker than that of ferric ions ($Fe^{2+}$ or $Fe^+$). The $NH_3$-TPD profile of $Cu_1Fe_1O_x$ MNs exhibits two weak desorption peaks associated with the medium and strong acid site, respectively, while the $Cu_2Fe_1O_x$ MNs exhibits only one weak desorption peak associated with strong acid site. It indicates the concentration of acid site of $CuFeO_x$ MNs significantly decrease with increasing the Cu/Fe ratio, which might be attributed to that more $Cu^+$ with weak acid strength in the $CuFeO_x$ MNs reduces the acidity. As for the $CO_2$- TPD profiles of MNs (Fig. 4b), it is observed that the $CO_2$-TPD profiles of MNs display a weak desorption peak and a strong broad desorption peak with the $T_M$ in region of 100–250℃ and 250–700 ℃, respectively, meaning that medium and strong base sites originated from $O^{2-}$ (Lewis base site, denoted as $\delta^-$) are dominant, along with the concentration order of $Fe_3O_4$ > $Cu_{0.5}Fe_1O_x$ > $Cu_1Fe_1O_x$ > $Cu_2Fe_1O_x$ (Table S2), which reveals that increasing the content of copper species also results in decreasing the basicity of $CuFeO_x$ MNs, probably due to that more $Cu^+$ occupying less O element leads to a decreased electron density around $O^{2-}$. In general, the as-prepared $CuFeO_x$ MNs have both acid site ($\delta^+$) and base site ($\delta^-$) on the surface, which is significantly affected by the Cu/Fe ratio, and will further affect the catalytic performance.

## Catalytic performance of $CuFeO_x$ MNs for catalytic PDO transformation

In order to demonstrate the anaerobic condition may be able to facilitate the catalytic transformation of PDO to LA over Cu-based catalysts, we first investigated the catalytic performance for $Cu_1Fe_1O_x$ MNs in the presence of $O_2$ and $N_2$ with pressure of 0.1−2 MPa at 140℃ and NaOH/PDO mole ratio of 2, as shown in Fig. 5a. It can see that lactic acid (LA), pyruvic acid (PA) and hydroxylacetone (HA) are the detected C3 products, while acetic acid (AA) and formic acid (FA) are the C1 and C2 product, respectively. As the $O_2$ pressures decrease from 2 to 0.1 MPa, the LA selectivity can be increased from 43.1% to 73.5% in spite of lowering the PDO conversion. However, the LA yields exhibit an increasing trend, revealing that lowering the $O_2$ pressure can significantly enhance the transformation of PDO to LA probably due to the inhibition of C3 product cleavage. According to this trend, the reaction is further carried out in the absence of $O_2$ ($N_2$ atmosphere). As expected, the LA selectivity can be further raised to 84.1% at 0.1 MPa $N_2$, which will be slightly enhanced to 86.8% and 87.5% at 1.0 and 2.0 MPa $N_2$, respectively. Although the PDO conversions at $N_2$ are lower than those at $O_2$, the obtained LA yields are higher at $N_2$, indicating that the $O_2$-free condition is proved to be beneficial for the catalytic transformation of PDO to LA. Considering that the polyols dehydrogenation reaction is

View Article Online
DOI: 10.1039/D0CY01733G

endothermic, it may be helpful for improving catalytic activity by elevating the reaction temperature. As shown in Fig. 5b, the catalytic activity of $Cu_1Fe_1O_x$ MNs remarkably depends on the temperature. Interestingly, the observed LA selectivity is first increased with raising the temperature and reaches the maximum of 94.5% at 160℃, comparable to that of noble metal/pressurized $O_2$ based route. Then, it is slightly decreased with further increasing the temperature from 160 to 200℃, probably due to the formation of more cleavage C1 and C2 products (formic and acetic acids). In addition to high LA yield, hydrogen is generated as a co-product with a nearly quantitative yield (Fig. S4 and Fig. S5), implying that apparently the oxidation of PDO proceeds in the absence of molecular oxygen and thus is accompanied by hydrogen production, thereby it is proposed to follow a similar reaction pathway as that of catalytic ethylene glycol transformation,[18] which can be written as (1):

$C_3H_8O_2$ (1,2-propanediol) + $H_2O \rightarrow C_3H_6O_3$ (lactic acid) + $2H_2$ (1).

Based on the above results, we can see that the catalytic transformation of PDO under anaerobic and basic aqueous conditions favors significant enhancement in LA selectivity as compared to that under pressurized $O_2$ condition and valuable $H_2$[34, 35] is produced simultaneously.

Table 2 and Fig. 5c show the results derived from the measurements of the catalytic performances of $O_2$-free catalytic PDO transformation over different Cu-based catalysts. In absence of catalyst, the PDO transformation can still proceed probably due to the promoting effect of alkali [23] but very slowly, giving only 3.2% PDO conversion after reacting for 8 h. No enhancement in PDO conversion is found for $Fe_3O_4$ MNs as compared to that without catalyst, indicating that they are inactive for this reaction. However, when $CuFeO_x$ MNs were used as catalysts, the PDO is efficiently and selectively transformed into LA, giving PDO conversion of > 58.1% and LA selectivity of > 90.7%, which is suggested that copper species in $CuFeO_x$ MNs can be the active component for promoting the reaction. Given the coexistence of $Cu^{2+}$ and $Cu^+$ species in $CuFeO_x$ MNs, it is worthy to give an insight into their effects on the catalytic performance. Herein, firstly, CuO and $Cu_2O$ with respectively, are selected to catalyze the PDO transformation.

Table 2 and Fig. 5c clearly show that the PDO conversion and TOF for $Cu_2O$ are much higher than those for CuO (66.5% and 420 $h^{-1}$ vs 38.3% and 270 $h^{-1}$), while the LA selectivity for $Cu_2O$ is lower than that for CuO (74.2% vs 83.5%). This result indicates that $Cu_2O$ with $Cu^+$ dominant is more active to catalyze the PDO conversion, while CuO with $Cu^{2+}$ alone shows higher LA selectivity, which can further be evidenced by that the $CuFe_2O_4$ with $Cu^{2+}$ alone (see the XPS and AES spectra in Fig. S6) displays high LA selectivity (88.6%) but with relative low PDO conversion (only 43.6%). Comparing with $CuFe_2O_4$, the $Cu_{0.5}Fe_1O_x$ MNs with similar Cu/Fe ratio and structure to $CuFe_2O_4$ displays enhanced PDO conversion and LA selectivity (58.1% and 92.1% vs 43.6% and 88.6%), implying that the combination of $Cu^+$ and $Cu^{2+}$ sites synergistically promote the reaction. Consequently, for $Cu_1Fe_1O_x$ MNs, by increasing the amount of $Cu^+$ and $Cu^{2+}$ species in $CuFeO_x$ MNs can further promote to the PDO conversion and LA selectivity to 72.6% and 94.5%, respectively. For comparison, when we used the oxidized $Cu_1Fe_1O_x$ MNs (denoted as o-$Cu_1Fe_1O_x$ MNs) with $Cu^{2+}$ species dominant (see the XPS and XAS spectra in Fig. S6) becomes less active (TOF of 760 $h^{-1}$) than the original $Cu_1Fe_1O_x$ MNs (TON of 1410 $h^{-1}$). On basis of the above results, it is

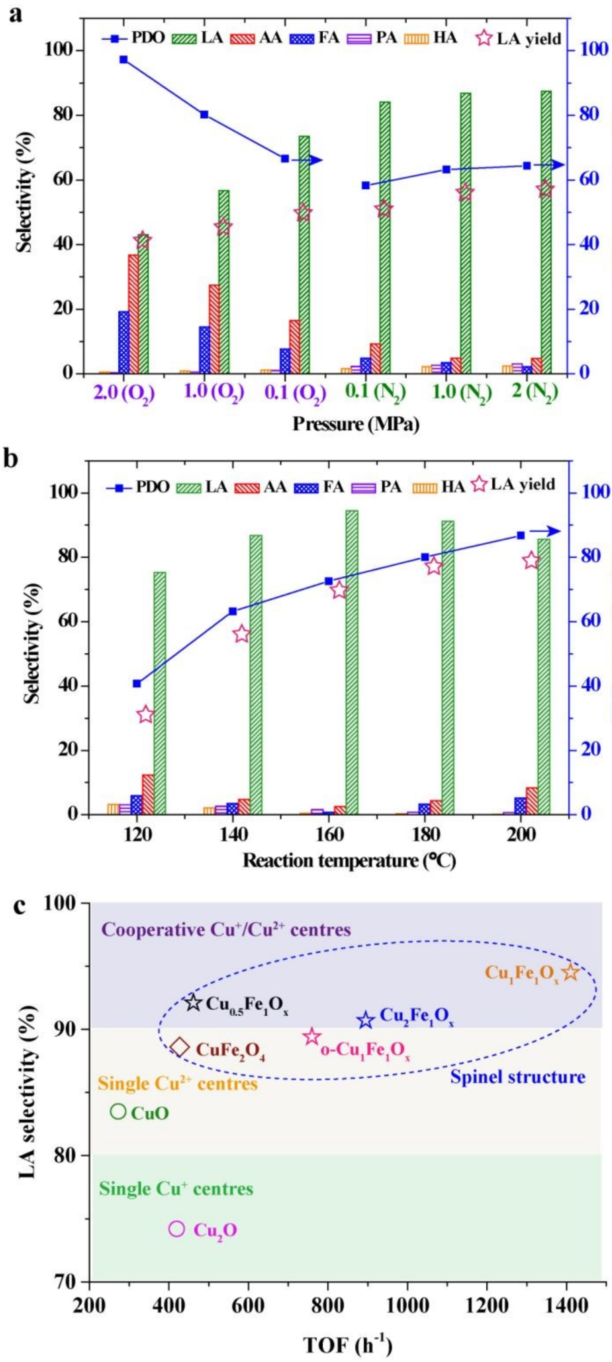

**Fig. 5.** Influences of $O_2$ and $N_2$ pressure (a) and temperature (b) on the PDO conversion and LA selectivity over Cu1Fe1Ox MNs. LA selectivity vs TOF over different Cu-based catalysts (c). Reaction conditions for a: $O_2$ or $N_2$ pressure = 0.1–2.0 MPa, reaction temperature = 140 ℃, PDO concentration = 0.2 M (40 mL), NaOH/PDO (mol/mol) = 2, catalyst loading = 0.06 g, reaction time = 8 h. Reaction conditions for b are similar to a expect alter the reaction temperature and keep N2 pressure of 1.0 MPa. Reaction conditions for c are similar to b except keep the reaction temperature of 160 ℃ and alter the type of catalyst. PDO = 1,2-propanediol, LA = lactic acid, AA = acetic acid, FA = formic acid, PA = pyruvic acid, HA = hydroxyacetone.

View Article Online
DOI: 10.1039/D0CY01733G

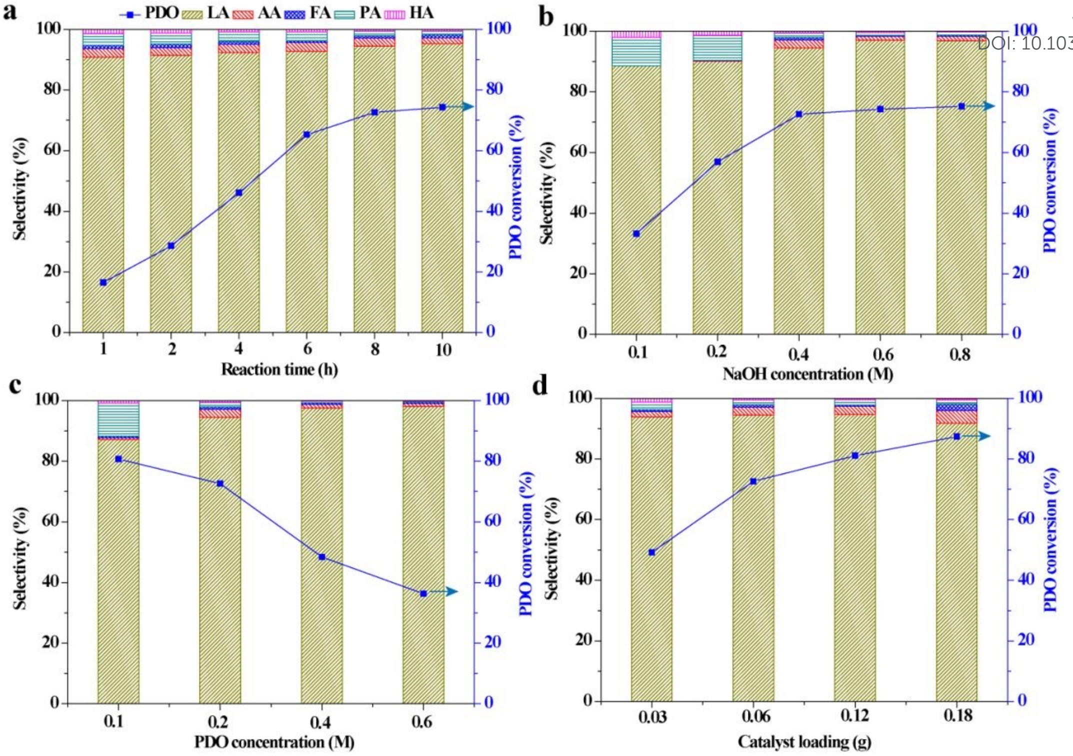

**Fig. 6.** The influences of other important reaction parameters (reaction time, NaOH concentration, PDO concentration and catalyst loading) on the catalytic performance of $Cu_1Fe_1O_x$ MNs. Reaction conditions: (a) reaction temperature = 160 ℃, $N_2$ pressure = 1.0 MPa, PDO concentration = 0.2 M (40 mL), NaOH/PDO (mol/mol) = 2, catalyst loading = 0.06 g; (b–d) reaction conditions are similar to (a) but just vary the corresponding reaction parameters and keep the reaction time for 8 h. PDO = 1,2-propanediol, LA = lactic acid, AA = acetic acid, FA = formic acid, PA = pyruvic acid.

suggested that the coexistence of $Cu^+$ and $Cu^{2+}$ dual sites on $CuFeO_x$ surface contribute to the enhanced activity and LA selectivity in the catalytic transformation of PDO over $CuFeO_x$ MNs. However, in spite of having highest copper amount, the $Cu_2Fe_1O_x$ MNs shows a slightly reduced PDO conversion (68.6%) and LA selectivity (90.7%) as compared to $Cu_1Fe_1O_x$ MNs, which may relate to their lower acid site ($\delta^+$) concentration and smaller surface area, exhibiting weaker interaction with PDO molecule. From Fig. 5c, through the comparison of LA selectivities among CuO, $CuFe_2O_4$, and o-$Cu_1Fe_1O_x$ with $Cu^{2+}$ species dominant, it turns out that both $CuFe_2O_4$ and o-$Cu_1Fe_1O_x$ MNs owing spinel structure favor higher TOFs, meaning the spinel structure of $CuFeO_x$ MNs is also important to facilitate the catalytic reaction. Therefore, the excellent catalytic performance of $CuFeO_x$ MNs for catalytic PDO transformation can be originated from the synergy between $Cu^+$ and $Cu^{2+}$ binary centres as well as the spinel structure.

The influences of other important parameters including reaction time, concentrations of PDO and NaOH, and catalyst loading on the catalytic performance were also investigated. Fig. 6a shows that prolonging the reaction time favors the increment of PDO conversion and lactic acid selectivity. High NaOH concentration (>0.4 M, Fig. 6b) significantly promotes the PDO conversion and lactic acid selectivity as compared to low NaOH concentration (<0.2 M). This is because alkali ($OH^-$) will participate in the polyols dehydrogenation reaction. However, an overdose of NaOH (>0.6 M) shows only a little enhancement in the PDO conversion and LA selectivity. So, the initial NaOH/PDO ratio was kept at 2 in order to improve the catalytic performance. In the case of PDO concentration effect (Fig. 6c), high PDO conversion but low LA selectivity is observed at low PDO concentration (0.1 M) probably due to the deeper catalytic conversion of PDO to pyruvic acid, while high PDO concentration (0.6 M) displays low PDO conversion but with high LA selectivity. Increasing the catalyst loading in the reaction (Fig. 6d) can obviously improve the PDO conversion but meanwhile cause serious C–C bond cleavage of C3 product leading to the declined LA selectivity. In general, the optimal reaction time, NaOH concentration, PDO concentration and catalyst loading can be fixed at 8 h, 0.4 M, 0.2 M, and 0.06 g, respectively.

## Reaction pathway and mechanism for catalytic PDO transformation

For the conventional "$O_2$-required" catalytic PDO oxidation over supported noble metal catalysts, it is generally supposed to follow a reaction network as depicted in Scheme 1c, in which the pathway of PDO → lactaldehyde → lactic acid is proposed as the desired pathway for LA production. However, as for the $O_2$-free catalytic transformation of PDO over spinel $CuFeO_x$ MNs, it is challenging to determine which pathway is preferable and how this can occur because either the terminal or secondary –OH group of PDO can be dehydrogenated first. Moreover, the intermediates can

View Article Online
DOI: 10.1039/D0CY01733G

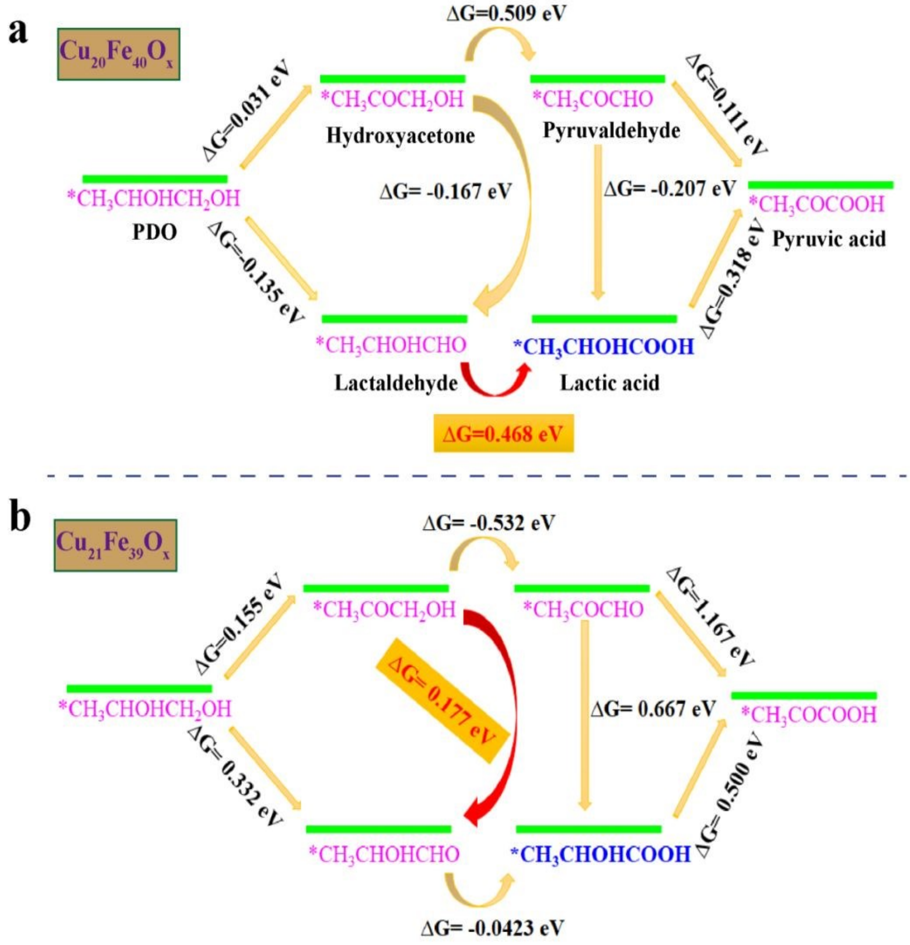

**Fig. 7.** Possible reaction routes based on DFT calculation for the $O_2$-free catalytic PDO conversion to LA over spinel $CuFe_2O_4$ surfaces with different Cu/Fe ratios of 20/40 and 21/39.

be transformed into each other reversely (Table 2). Therefore, herein, DFT calculations are employed to identify the favourite pathway for the catalytic PDO transformation over $CuFeO_x$ MNs, in which the spinel $CuFe_2O_4$ (311) plane is designed as the model surface because the synthesized $CuFeO_x$ MNs have the similar structure to $CuFe_2O_4$ (XRD and HRTEM). Here, two types of $CuFe_2O_4$ surfaces with different Cu/Fe atom ratios of 20/40 and 21/39, designated as $Cu_{20}Fe_{40}O_x$ and $Cu_{21}Fe_{39}O_x$, respectively, are built as the models in view of the surface content significantly affecting their catalytic activity.

Fig. 7a depicts the reaction energy diagram for the catalytic PDO conversion over the $Cu_{20}Fe_{40}O_x$ surface, in which the Cu/Fe ratio is 1:2. Before reaction, PDO is considered to be first adsorbed on the $Cu_{20}Fe_{40}O_x$ surface to form an intermediate state ($*CH_3CHOHCH_2OH$, where the asterisk indicates the catalyst). It clearly shows that the energy for the dehydrogenation of PDO to lactaldehyde ($*CH_3CHOHCHO$) ($\Delta G = –0.135$ eV) through breaking the C–H bond of terminal alkoxy species is lower than that to hydroxyacetone ($*CH_3CHOCHOH$) ($\Delta G = 0.031$ eV) through breaking the C–H bond of secondary alkoxy species, indicating that the conversion of PDO to LA over $Cu_{20}Fe_{40}O_x$ surface favours following the reaction path of initial dehydrogenation of PDO to lactaldehyde, which is then transformed to lactic acid ($*CH_3CHOHCOOH$). The conversion of lactaldehyde to LA over $Cu_{20}Fe_{40}O_x$ surface is the rate determining step due to its requirement of high energy. However, as for $Cu_{21}Fe_{39}O_x$ surface with higher Cu ratio (Fig. 7b), it favours the initial dehydrogenation of PDO to hydroxyacetone ($\Delta G = 0.155$ eV), and the tautomeric into lactaldehyde is only 0.177 eV. Nevertheless, the LA formation from the lactaldehyde conversion is more favourable than from the pyruvaldehyde conversion via Cannizaro reaction due to the low energy of −0.0423 eV. As a result, the tautomeric equilibrium of hydroxyacetone to lactaldehyde can be the rate determining step for the LA production over the $Cu_{21}Fe_{39}O_x$ surface. These data are also well agreed with the experimental results for that the heavily decreased barrier of determination step can greatly enhance the reaction kinetics, and reduce the reaction temperature. Therefore, a high yield of LA has been observed at low temperature of 160℃.Moreover, the bond distance of C−H and O−H near Cu or Fe atoms, as well as their atomic charge are calculated, as listed in Table S5. The secondary O−H distance of PDO is not changed both on $Cu_{20}Fe_{40}O_x$ or $Cu_{21}Fe_{39}O_x$, but the charge of O is enhanced on $Cu_{21}Fe_{39}O_x$, which could enhance the adsorption of H, resulting high conversion energy for the first step from PDO to

View Article Online
DOI: 10.1039/D0CY01733G

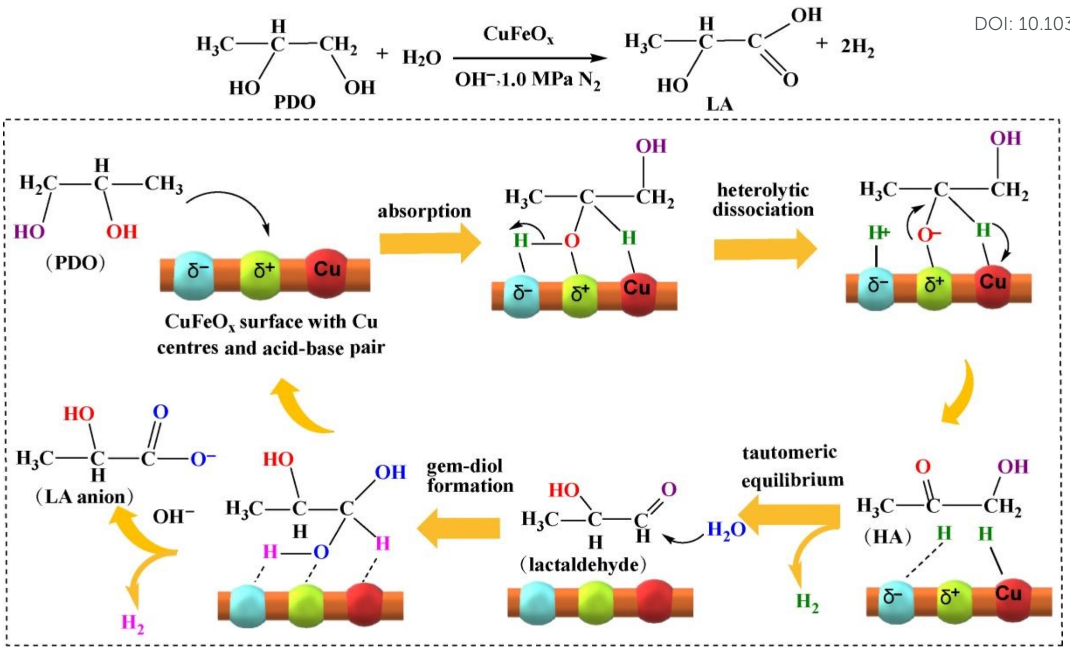

**Scheme 2.** Proposed reaction mechanism for $O_2$-free catalytic PDO conversion to LA over $CuFeO_x$ MNs.

hydroxyacetone (Scheme 1c). For the step from hydroxyacetone to lactaldehyde, the change of O−H can be neglected. And the charge of O at C=O on $Cu_{20}Fe_{40}O_x$ is lower than that on $Cu_{21}Fe_{39}O_x$ sample, which means that the O at C=O on $Cu_{21}Fe_{39}O_x$ cannot accept more electrons from the added H, leading to a higher barrier for the step of hydroxyacetone to lactaldehyde on $Cu_{21}Fe_{39}O_x$. More than that, the Coulomp interaction between C and H on $Cu_{20}Fe_{40}O_x$ is lower than it on $Cu_{21}Fe_{39}O_x$, which also indicates that the barrier should be lower on $Cu_{20}Fe_{40}O_x$. For the reaction from lactaldehyde to lactate, the positive charge of C of C−H on $Cu_{21}Fe_{39}O_x$ is much higher than that on $Cu_{20}Fe_{40}O_x$, which can strong attract the negative charged O atoms, therefore, the barrier is very lower for this reaction on $Cu_{21}Fe_{39}O_x$.

In general, through the DFT calculations we can find that the highly selective LA formation over spinel $CuFe_2O_4$ surface originates from the conversion of lactaldehyde instead of pyruvaldehyde. The intermediate lactaldehyde can be formed by the catalytic dehydrogenation of the primary −OH group of PDO, or by tautomeric equilibrium of hydroxyacetone, depending on the surface Cu/Fe ratio of $CuFe_2O_4$. As for the actual $CuFeO_x$ MNs, since their surface Cu/Fe atom ratios are higher than 1/2, as the XPS analysis (Table 1), it is supposed to follow a favourite pathway similar to that of $Cu_{21}Fe_{39}O_x$ surface (Fig. 6b) to generate LA. Moreover, the characteristic intermediate hydroxyacetone is detected in the reaction, indicating the dehydrogenation of secondary −OH group of PDO likely occurs. The production of acetic and formic acids suggests the side reaction of the C–C bond cleavage of pyruvaldehyde can also occur due to its easy dissociation to form acetic and formic acids (Table S6). This result is consistent with the easy formation of pyruvaldehyde in the simulative reaction routes over $Cu_{21}Fe_{39}O_x$ surface. Thus, the $CuFeO_x$ MNs based catalytic PDO transformation is suggested to follow a dominant pathway of PDO → hydroxyacetone → lactaldehyde → lactic acid for LA production, but how can it undergo?

It is reported that for the oxidative dehydrogenation of ethanol to acetaldehyde over $CuFe_2O_4$, it is supposed to follow the a mechanism with heterolytic dissociation of the O–H and C–H bonds on the acid–base [Cu–O] pair.[20] Moreover, the acid–base sites of catalyst can accelerate the cleavage of O–H bond in the $O_2$-free dehydrogenation of alcohols.[36] Inspired by these, the $CuFeO_x$ MNs with a large number of acid-base pairs (Table S2) can be considered as the acid-base [$\delta^+$–$\delta^-$] pair. Based on these, a possible scheme that may appear best to explain the mechanism of $CuFeO_x$ MNs based $O_2$-free catalytic conversion of PDO to LA is shown in Scheme 2. First of all, PDO is supposed to be absorbed on the $CuFeO_x$ surface, where the secondary –OH group would like to interact with the acid-base sites, while the α–C–H likely interacts with the copper centres.[36, 37] It is then dehydrogenated to generate a hydroxyacetone with a quantitative $H_2$ release, which further transforms into lactaldehyde via the tautomeric equilibrium. The lactaldehyde can be in equilibrium with its *gem*-diol via the interaction with water,[16] which is further dehydrogenated to produce LA with another $H_2$ release, and it is rapidly deprotonated to lactate by the added base under alkaline condition.[17]

In this reaction, LA can be selectively transformed to pyruvic acid catalyzed by $Cu_1Fe_1O_x$ MNs (Table S6), which can be further dissociated into acetic acid (Table S6), a stable C2 product detected in our experiment, and carbonic acid, a possible C1 product which is not included in this study. No conversion is observed when using $Cu_1Fe_1O_x$ MNs to catalyze the acetic acid and formic acid (Table S6), suggesting that these two products are rather stable. Previous reports show acetic acid and formic acid could be derived from the cleavage of pyruvaldehyde.[5, 38] Table S6 shows acetic acid and formic

View Article Online
DOI: 10.1039/D0CY01733G

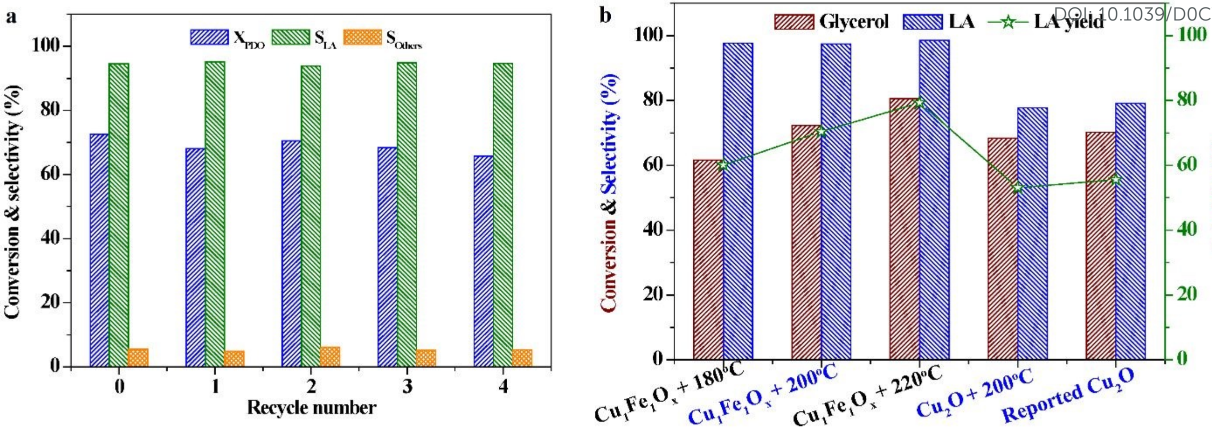

**Fig. 8.** Recycling performance of $Cu_1Fe_1O_x$ MNs (d). Catalytic performance for catalytic hydrothermal conversion of glycerol to LA over $Cu_1Fe_1O_x$ MNs, with $Cu_2O$ as comparison (e). Reaction conditions for c, d, e: $N_2$ pressure = 1 MPa, reaction temperature = 160℃, PDO concentration = 0.2 M (40 mL), NaOH/PDO (mol/mol) = 2, catalyst loading = 0.06 g, reaction time = 8 h; Reaction conditions for f: reaction temperature = 180–220℃, glycerol concentration = 1.08 M (30 mL), NaOH concentration = 1.2 M, $N_2$ pressure = 1.4 MPa, catalyst loading = 0.2 g, reaction time = 6 h. $X_{PDO}$ = conversion of 1,2-propanediol, $S_{LA}$ = lactic acid selectivity, $S_{others}$ = selectivity of other products.

acid can be observed when using $Cu_1Fe_1O_x$ MNs to catalyze pyruvaldehyde, while only acetic acid is observed when it catalyzes pyruvic acid. Thus, formic acid, another C1 product, is probably derived from the C−C bond cleavage of pyruvaldehyde, and acetic acid (C2 product) can be derived from the dissociation of pyruvaldehyde or pyruvic acid. Comparing with CuO and $Cu_2O$, $Cu_1Fe_1O_x$ MNs is more favorable for LA production even using hydroxyacetone as raw material, accompanying with lower C1 and C2 product selectivity (Table S6). Moreover, $Cu_1Fe_1O_x$ MNs displays lower catalytic dissociation of pyruvic acid to acetic acid. The results indicate the $Cu_1Fe_1O_x$ MNs shows lower dissociation of C3 products. Furthermore, the conversion of LA to pyruvic acid over $Cu_1Fe_1O_x$ MNs is much higher than that over CuO and $Cu_2O$, indicating that the $Cu_1Fe_1O_x$ MNs has superior dehydrogenation capacity. In general, owing to the coexistence of $Cu^+$ and $Cu^{2+}$ dual sites and the spinel structure, the $CuFeO_x$ MNs is highly active and selective for catalytic transformation of PDO to LA under anaerobic and basic aqueous conditions.

## Recycling performance of $CuFeO_x$ MNs

Fast hot catalyst filtration experiment was used to determine copper species on $CuFeO_x$ MNs were the real active sites.[39] After the reaction was conducted for 4 h, the conversion of PDO exceeds 45%. No further PDO conversion in the filtrate is found after removal of the catalyst in the oxidation over $Cu_1Fe_1O_x$ MNs (Fig. S7a), indicating the true heterogeneous catalysis. A trace amount of copper and iron elements (less than 2 ppm) was determined in the filtrate by ICP-AES after reaction, suggesting that the catalytic reactivity by the leaching could be almost excluded in the present catalytic conditions. Moreover, the reusability of $Cu_1Fe_1O_x$ MNs was performed under the optimized catalytic conditions. After reaction, the spent $Cu_1Fe_1O_x$ MNs were easily separated from the reaction mixture by using an external magnet due to their good magnetic property (Fig. S7b), washed with ethanol three times, and further reused directly. The $Cu_1Fe_1O_x$ MNs remains high activity after 5 cycles in spite of a slight decrease in the PDO conversion (Fig. 8a), probably due to a little amount of copper species leaked from $Cu_1Fe_1O_x$ MNs (ICP-AES analysis, Table S3). The XRD pattern (Fig. S8a) of the spent $Cu_1Fe_1O_x$ MNs displays two new characteristic peaks of cuprite ($Cu_2O$, JPFDS05-0667) as compared to the fresh one, indicating the exposed $Cu^+$ species of the spent catalyst. However, the TEM and HRTEM images (Fig. S8b-c), element-mapping (Fig. S8e-h) show that the size, morphology, crystal structure, chemical composition of the spent $Cu_1Fe_1O_x$ MNs remains unchanged, indicating its good recycling performance and stability.

## Extension of $CuFeO_x$ MNs for catalytic glycerol and ethylene glycol transformations

The catalytic hydrothermal conversion of glycerol has been also believed as a green strategy for LA production. Previous work has shown that $Cu_2O$ is active for catalyzing the glycerol conversion to LA, giving 70.2% glycerol conversion and 79.2% LA selectivity at NaOH/glycerol ratio of 1 and 200℃ for 6 h.[23] Considering that $CuFeO_x$ MNs is more selective than $Cu_2O$ for catalytic transformation of PDO to LA, we tried to use the optimal $Cu_1Fe_1O_x$ MNs to catalyze hydrothermal conversion of glycerol under the same conditions, with $Cu_2O$ as comparison, aiming at enhancing the LA selectivity. The results are shown in Fig. 8b. It can see that the $Cu_1Fe_1O_x$ MNs displays 72.3% glycerol conversion, slightly higher than that for $Cu_2O$ (68.4%), whereas the LA selectivity is boosted to 97.8%, much higher than that for $Cu_2O$ (77.7%), accompanied with a quantitative yield of $H_2$ (0.95, Fig. S5). By increasing the reaction temperature to 220℃ can further raise the glycerol conversion to 80.5% and still maintain high LA selectivity of 98.5%. In addition to high catalytic performance in catalytic

View Article Online
DOI: 10.1039/D0CY01733G

glycerol transformations, it is found that $Cu_1Fe_1O_x$ MNs can also promote the highly selective transformation of ethylene glycol into glyceric acid (87.4% conversion and 97.8% selectivity, Table S4) at 160 ℃. The results demonstrate that the spinel $CuFeO_x$ MNs with coexistence of Cu(I) and Cu(II) dual sites is an alternative efficient catalyst for catalytic polyols transformation to value-added carboxyl acids under anaerobic and basic conditions.

## Experimental section

### Materials

Benzyl ether (95%), oleylamine (C18： 80-90%), Iron(III) acetylacetonate (98%) and copper(II) acetylacetonate (97%) were of reagent grade and purchased from Shanghai Aladdin Biochemical Technology Co., Ltd. Absolute ethanol (≥ 99.5%), hexane (> 99%), 1,2-propanediol (PDO, >99%), lactic acid (LA, 90%), pyruvic acid (98%), hydroxyacetone (95%), formic acid (>99%), and acetic acid (>99%) were of reagent grade and bought from Sinopharm Chemical Reagent Co., Ltd. All the reagents are used without any purification.

### Preparation of $CuFeO_x$ magnetic nanoparticles (MNs)

The synthesis of $CuFeO_x$ MNs was followed by the procedure adopted from the synthesis of monodispersed $Fe_3O_4$ nanoparticles,[24] and was modified slightly to make $CuFeO_x$ MNs here. The as prepared $CuFeO_x$ MNs with different molar ratios of Cu/Fe are denoted as $Cu_aFe_1O_x$, of which the letters represent the molar ratio of each element. For example, $Cu_1Fe_1O_x$ means the molar ratio of Cu/Fe is 1:1, which is synthesized by the following procedure. Typically, 4 mmol of $Fe(acac)_3$ and 4 mmol $Cu(acac)_2$ was added into a 250 mL flask and dissolved in a mixture of 20 mL benzyl ether, 100 mL ethanol and 30 mL oleylamine. The solution was heated at 110°C for 1 h with strong stirring, and was quickly heated to 300°C for 2 h. The precipitate was collected by centrifugation and was washed several times with hexane and ethanol, respectively. Monodispersed $Fe_3O_4$, $Cu_{0.5}Fe_1O_x$, and $Cu_2Fe_1O_x$ MNs were prepared as comparison.

### Characterizations

Nitrogen adsorption-desorption isotherms were measured at −196 ℃ by a NOVA 2000e physical adsorption apparatus. The specific surface areas ($S_{BET}$) of the samples were determined by BET method. The actual contents of Cu and Fe were determined by inductively coupled plasma (ICP) technique (VISTA-MPX).

The identification of crystal phases of $CuFeO_x$ MNs is performed by X-ray powder diffraction (XRD), which were recorded on a diffractometer (D8 super speed Bruke-AEX Company, Germany) with Cu Ka (k = 1.54056 Å) radiation in the range of 20–80°.

Transmission electron microscopy (TEM) images were performed on a microscopy (Tecnai 12) operated at an acceleration voltage of 120 KV. High resolution transmission electron microscopy (HRTEM) images were obtained on a microscopy (Tecnai G2 F30) operated at an acceleration voltage of 200 KV. Particularly, the samples were prepared on Ni grid.

X-ray photoelectron spectra (XPS) of $CuFeO_x$ MNs were recorded on an ESCALAB 250 spectrometer (PHI5000 Versa Probe,) using Al Ka radiation at 1486.6 eV. The resolution of the XPS is ± 0.1 eV. The binding energies of Cu and Fe were calculated with respect to C 1s peak of contaminated carbon at 284.6 eV.

The reduction behaviors of the catalysts were investigated by temperature programmed reduction (TPR) technique using a mixed $H_2/N_2$ flow (5:95, v/v) of 30 mL $min^{-1}$ and 0.05 g of the calcined catalysts at a temperature ramp of 10 ℃ $min^{-1}$ from 50 to 400℃. $H_2$ consumption was determined by analyzing the effluent gas with a thermal conductivity detector. The calcined catalysts were preheated in air at 400 ℃ before the TPR measurement in order to eliminate the adsorbed water.

Acidic and basic properties of catalysts were analyzed by $CO_2$ and $NH_3$ temperature-programmed desorption (TPD) on a fixed-bed continuous flow microreactor at atmospheric pressure. For basicity or acidity evaluation by $CO_2$-TPD or $NH_3$-TPD, 0.1 g sample was dried at 400℃ for 1 h in helium. Then, $CO_2$ or $NH_3$ $CO_2$ was introduced to the sample at 100℃ for 1 h. After purging with helium (30 mL $min^{-1}$) at 100℃ for 0.5 h to remove the weakly adsorbed $CO_2$ or $NH_3$ until the baseline of TCD signals stabilized, the TPD experiment was carried out at a linear heating rate of 10℃ $min^{-1}$ from 100 to 800℃.

CO pulse chemisorption was used to calculate the dispersion of surface copper,[40] which was conducted using a chemisorption module of the Micromeritics AutoChem II 2910 instrument. Prior to the experiment, the sample was first reduced at 350°C by 10 vol% $H_2$/He with a flow rate of 10°C $min^{-1}$ for 1 h and then cooled to 60℃ under a high purity He flow rate of 10 mL $min^{-1}$. Afterward, as the temperature declined to 60℃, successive pulses of CO were injected, using He as the carrier gas (10 mL $min^{-1}$) until the baseline is balanced. Metal dispersion (D%, eq 1) was calculated on the basis of the results of CO pulse chemisorption at 60℃ (Table 1):

$$D\% = \frac{V_{Chem}/22414 \times SF \times M_W}{\mathrm{m}_{cat}} \times 100 \qquad (2)$$

where $V_{chem}$, SF, $M_W$, and $m_{cat}$ are the amount of CO adsorption ($cm^{-3}$), stoichiometry factor, atomic weight of metal (g $mol^{-1}$), and weight of sample (g). SF is the stoichiometric factor, which is assumed as 1:1 for CO:Cu. The obtained surface metallic $Cu^0$ dispersion can be considered as the dispersion of $Cu^+$ and $Cu^{2+}$ on $CuFeO_x$ MNs because the metallic $Cu^0$ was obtained by the reduction of $Cu^+$ and $Cu^{2+}$.

### Catalytic Test

The catalytic oxidation of PDO was performed in a 250 mL capacity stainless steel autoclave equipped with a magnetically driven impeller. The autoclave was charged with appointed amounts of PDO, water, sodium hydroxide, and catalyst. First, the autoclave was purged with $N_2$ for 30 min. The reaction was carried out at a given temperature with the stirring speed of 800 rpm, at which the external diffusion could be eliminated (Fig. S1). Moreover, intraparticle diffusion limitation for the reaction was determined on basis of Weisz–Prater criterion [41] (see supporting information), which was suggested that intraparticle diffusion limitation could also be negligible under our reaction conditions. After reacting for certain time, 1 mL of mother liquid was sampled from the autoclave. The concentration of remained PDO was analyzed on a gas phase chromatograph equipped with a PEG-20M packed capillary column (0.25 mm × 30 m) and FID by the internal standard method with n-butanol as the internal standard. The liquid products were analyzed on a Agilent HPLC system equipped with a strong cation hydrogen exchange column (Carbomix H-NP, 7.8 mm × 300 mm) and a UV detector (λ = 210 nm) at 55°C. Before analysis, the reaction mixture was acidified with hydrochloric acid (12 M) to the pH value of 2–3. Sulphuric acid (5 mM) was used as a mobile phase with a flow rate of 0.8 mL $min^{-1}$. The concentrations of the products were analyzed by the external standard method. Gas products were collected by Tedlar bag after reaction and cooling down to room temperature, in which $H_2$ was determined by a gas phase chromatograph (Test Instrument GC-2030) with a TDX-01 carbon molecular sieve packed column and TCD detector under $N_2$ carrier. The conversion of PDO, selectivity of products and turnover frequency (TOF) are the factors used to evaluate the catalyst performance. They are each defined by the following equations.

$$Conversion\ (\%)\ = \frac{amount\ of\ PDO\ \ converted\ (mol)}{total\ amount\ of\ PDO\ \ \ (mol)} \times 100 \qquad (3)$$

$$Selectivity\ (\%)\ = \frac{moles\ of\ carbon\ in\ a\ specific\ product}{moles\ of\ carbon\ in\ all\ products} \times 100 \quad (4)$$

$$TOF(h^{-1}) = \frac{converted\ PDO\ (mol)}{surface\ copper\ in\ catalyst\ (mol)} \div\ time\ (h) \qquad (5)$$

### DFT calculation method

The corresponding detailed descriptions about the DFT calculation are listed in supporting information. It should be noted that the aqueous solution effect is not considered in this work since many previous work demonstrate that the Gibbs free energy cannot be heavily influenced by solution.[42-44]

## Conclusions

Novel spinel $CuFeO_x$ MNs with $Cu^+/Cu^{2+}$ dual sites are controllably synthesized by the high-temperature organic phase synthesis method. By tuning the Cu/Fe ratio can facilely tailor their particle size and surface $Cu^+/Cu^{2+}$ ratio and acid-base sites. The $CuFeO_x$ MNs are highly active and selective for catalyzing the PDO transformation to LA in absence of $O_2$ and basic aqueous solution, giving optimal LA selectivity of 94.5% and PDO conversion of 72.6% at 160℃ for 8 h, much higher than that for CuO or $Cu_2O$ with $Cu^{2+}$ or $Cu^+$ single sites. The $CuFeO_x$ MNs can be extended to catalyze the selective conversion of glycerol to LA and ethylene glycol to glyceric acid. This high catalytic performance of $CuFeO_x$ MNs for catalytic bio-based polyols can be attributed to the synergy between $Cu^+$ and $Cu^{2+}$ binary centres. DFT calculations and experimental results suggest the $CuFeO_x$ MNs likely follows a favorable pathway of PDO → hydroxyacetone → lactaldehyde → LA for the catalytic transformation of PDO into LA. The $CuFeO_x$ MNs display good recycling performance and can be facilely recovered by magnetic separation. This work provides an alternative strategy and new insights for enhancing the catalytic transformation of bio-based polyols to carboxyl acids over non-precious metal based catalyst.

## Conflicts of interest

There are no conflicts to declare.

## Acknowledgements

This work was financially supported by the National Natural Science Foundation of China (No. 21606112), China Postdoctoral Fundation Committee (No. 2019T120400), Programs of Senior Talent Foundation of Jiangsu University (No. 15JDG137) and Youth Talent Cultivation Plan of Jiangsu University.

## Notes and references

1. Z. Zhang and G. W. Huber, *Chem. Soc. Rev.*, 2018, **47**, 1351-1390.
2. S. Dutta and K. C. W. Wu, *Green Chem.*, 2014, **16**, 4615-4626.
3. M. Besson, P. Gallezot and C. Pinel, *Chem. Rev.*, 2014, **114**, 1827-1870.
4. R. Datta and M. Henry, *J. Chem. Technol. Biot.*, 2006, **81**, 1119-1129.
5. D. J. Chadderdon, L. Xin, J. Qi, B. Brady, J. A. Miller, K. Sun, M. J. Janik and W. Li, *ACS Catal.*, 2015, **5**, 6926-6936.
6. L. Prati and M. Rossi, *J. Catal.*, 1998, **176**, 552-560.
7. N. Dimitratos, J. A. Lopez-Sanchez, S. Meenakshisundaram, J. M. Anthonykutty, G. Brett, A. F. Carley, S. H. Taylor, D. W. Knight and G. J. Hutchings, *Green Chem.*, 2009, **11**, 1209-1216.
8. Y. H. Feng, H. B. Yin, D. Z. Gao, A. L. Wang, L. Q. Shen and M. J. Meng, *J. Catal.*, 2014, **316**, 67-77.
9. Y. Feng, H. Yin, A. Wang, D. Gao, X. Zhu, L. Shen and M. Meng, *Appl. Catal. A: Gen.*, 2014, **482**, 49-60.
10. Y. Ryabenkova, Q. He, P. J. Miedziak, N. F. Dummer, S. H. Taylor, A. F. Carley, D. J. Morgan, N. Dimitratos, D. J. Willock, D. Bethell, D. W. Knight, D. Chadwick, C. J. Kiely and G. J. Hutchings, *Catal. Today*, 2013, **203**, 139-145.
11. W. Xue, Y. Feng, H. Yin, S. Liu, A. Wang and L. Shen, *J. Nanosci. Nanotechnol.*, 2016, **16**, 9621-9633.
12. F. Du, H. Wang, X. Jin, W. Deng, C. Li, Z. Ren, H. Yan and B. Yin, *Catal. Lett.*, 2019, **149**, 1037-1045.
13. W. Xue, H. Yin, Z. Lu, Y. Feng, A. Wang, S. Liu, L. Shen and X. Jia, *Catal. Lett.*, 2016, **146**, 1139-1152.
14. Y. Feng, H. Yin, A. Wang and W. Xue, *J. Catal.*, 2015, **326**, 26-37.
15. W. Xue, H. Yin, Z. Lu, A. Wang, S. Liu and L. Shen, *J. Nanosci. Nanotechnol.*, 2018, **18**, 3362-3372.
16. E. Balaraman, E. Khaskin, G. Leitus and D. Milstein, *Nat. Chem.*, 2013, **5**, 122-125.
17. H. Li and M. B. Hall, *J. Am. Chem. Soc.*, 2014, **136**, 383-395.
18. T. van Haasterecht, T. W. van Deelen, K. P. de Jong and J. H. Bitter, *Catal. Sci. Technol.*, 2014, **4**, 2353-2366.
19. M. B. Griffin, A. A. Rodriguez, M. M. Montemore, J. R. Monnier, C. T. Williams and J. W. Medlin, *J. Catal.*, 2013, **307**, 111-120.
20. L. Y. Dolgykh, I. L. Stolyarchuk, L. A. Staraya, I. V. Vasylenko,

View Article Online
DOI: 10.1039/D0CY01733G

Y. I. Pyatnitsky and P. E. Strizhak, *Theor. Exp. Chem.*, 2015, **51**, 230-235.
21. H. Lee, J. C. Jung, H. Kim, Y.-M. Chung, T. J. Kim, S. J. Lee, S.-H. Oh, Y. S. Kim and I. K. Song, *Catal. Lett.*, 2008, **124**, 364-368.
22. T. Mathew, S. Malwadkar, S. Pai, N. Sharanappa, C. P. Sebastian, C. V. V. Satyanarayana and V. V. Bokade, *Catal. Lett.*, 2003, **91**, 217-224.
23. D. Roy, B. Subramaniam and R. V. Chaudhari, *ACS Catal.*, 2011, **1**, 548-551.
24. S. Sun, H. Zeng, D. B. Robinson, S. Raoux, P. M. Rice, S. X. Wang and G. Li, *J. Am. Chem. Soc.*, 2004, **126**, 273-279.
25. W. Zhang, B. Quan, C. Lee, S.-K. Park, X. Li, E. Choi, G. Diao and Y. Piao, *ACS Appl. Mater. Interfaces*, 2015, **7**, 2404-2414.
26. L. Wang, D. C. Bock, J. Li, E. A. Stach, A. C. Marschilok, K. J. Takeuchi and E. S. Takeuchi, *ACS Appl. Mater. Interfaces*, 2018, **10**, 8770-8785.
27. Y. Feng, A. Wang, H. Yin, X. Yan and L. Shen, *Chem. Eng. J.*, 2015, **262**, 427-435.
28. T. Mathew, S. Shylesh, B. M. Devassy, M. Vijayaraj, C. V. V. Satyanarayana, B. S. Rao and C. S. Gopinath, *Appl. Catal. A: Gen.*, 2004, **273**, 35-45.
29. P. Liu and E. J. M. Hensen, *J. Am. Chem. Soc.*, 2013, **135**, 14032-14035.
30. Y. Su, H. Jiang, Y. Zhu, X. Yang, J. Shen, W. Zou, J. Chen and C. Li, *J. Mater. Chem. A*, 2014, **2**, 7281-7287.
31. K.-i. Shimizu, K. Kon, K. Shimura and S. S. M. A. Hakim, *J. Catal.*, 2013, **300**, 242-250.
32. Y. Feng, W. Xue, H. Yin, M. Meng, A. Wang and S. Liu, *RSC Adv.*, 2015, **5**, 106918-106929.
33. F. Jiang, L. Zeng, S. Li, G. Liu, S. Wang and J. Gong, *ACS Catal.*, 2015, **5**, 438-447.
34. Y. Qin, H. Li, J. Lu, Y. Feng, F. Meng, C. Ma, Y. Yan and M. Meng, *Appl. Catal. B: Environ.*, 2020, **277**, 119254.
35. Y. Qin, H. Li, J. Lu, F. Meng, C. Ma, Y. Yan and M. Meng, *Chem. Eng. J.*, 2020, **384**, 123275.
36. H. Chen, S. He, M. Xu, M. Wei, D. G. Evans and X. Duan, *ACS Catal.*, 2017, **7**, 2735-2743.
37. F. Wang, R. Shi, Z.-Q. Liu, P.-J. Shang, X. Pang, S. Shen, Z. Feng, C. Li and W. Shen, *ACS Catal.*, 2013, **3**, 890-894.
38. Y. Feng, W. Li, M. Meng, H. Yin and J. Mi, *Appl. Catal. B: Environ.*, 2019, **253**, 111-120.
39. R. A. Sheldon, M. Wallau, I. W. C. E. Arends and U. Schuchardt, *Accounts Chem. Res.*, 1998, **31**, 485-493.
40. S. Srivastava, P. Mohanty, J. K. Parikh, A. K. Dalai, S. S. Amritphale and A. K. Khare, *Chinese J. Catal.*, 2015, **36**, 933-942.
41. S. T. Oyama, X. Zhang, J. Lu, Y. Gu and T. Fujitani, *J. Catal.*, 2008, **257**, 1-4.
42. H. Niu, X. Wang, C. Shao, Z. Zhang and Y. Guo, *ACS Sustain. Chem. Eng.*, 2020, **8**, 13749-13758.
43. J. H. Montoya, C. Tsai, A. Vojvodic and J. K. Nørskov, *ChemSusChem*, 2015, **8**, 2180-2186.
44. D. Rao, H. Yang, X. Shen, X. Yan and G. Qiao, *Phys. Chem. Chem. Phys.*, 2019, **21**, 10895-10901.

View Article Online
DOI: 10.1039/D0CY01733G

# Table of contents entry

Synergy between Cu(I) and Cu(II) sites in spinel $CuFeO_x$ magnetic nanoparticles contributes to the significant enhancement in catalytic 1,2-propanediol transformation into lactic acid.